J|A|C|S
ARTICLES
Published on Web 06/22/2006

Molecular Understanding of Alumina Supported Single-Site Catalysts by a Combination of Experiment and Theory

Jérôme Joubert,[†] Françoise Delbecq,[†] Philippe Sautet,*[,†] Erwan Le Roux,[‡] Mostafa Taoufik,[‡] Chloé Thieuleux,[‡] Frédéric Blanc,[‡] Christophe Copéret,[‡] Jean Thivolle-Cazat,[‡] and Jean-Marie Basset*[,‡]

Contribution from the Laboratoire de Chimie (UMR 5182 CNRS/ENS), Ecole Normale Supérieure de Lyon, 46 Allée d'Italie, F-69364 Lyon Cedex 07, France, and the Laboratoire de Chimie Organométallique de Surface (UMR 9986 CNRS/ESCPE Lyon), ESCPE Lyon, F-308-43 Boulevard du 11 Novembre 1918, F-69616 Villeurbanne Cedex, France

Received March 10, 2006; E-mail: Philippe.Sautet@ens-lyon.fr; basset@cpe.fr

Abstract: The nature and structure of grafted organometallic complexes on γ-alumina are studied from a combination of experimental data (mass balance analysis, IR, NMR) and density functional theory calculations. The chemisorptive interactions of two complexes are analyzed and compared. The reaction of $[Zr(CH_2tBu)_4]$ with alumina dehydroxylated at 500 °C gives $\{[(Al_sO)_2Zr(CH_2tBu)]^+[(tBuCH_2)(Al_s)]^-\}$, a bisgrafted cationic complex as major surface species. The DFT calculations show that the reaction with surface hydroxyls is very exothermic and that alkyl transfer on Al atoms is favored. In contrast, $[W(\equiv CtBu)(CH_2tBu)_3]$ reacts with an alumina treated under identical conditions to give selectively a monografted neutral surface complex, $[(Al_sO)W(\equiv CtBu)(CH_2tBu)_2]$. This was inferred by the evolution of 1 equiv of $tBuCH_3$ per grafted W and the presence of remaining hydroxyls. The calculations show that the reaction of $[W(\equiv CtBu)(CH_2tBu)_3]$ with surface hydroxyls is in fact less exothermic and has a considerably higher activation barrier than the one of the Zr complex. Additionally, the transfer of an alkyl ligand onto an adjacent Al center is disfavored, and hence cationic species are not formed. Some ligands of this monoaluminoxy surface complex interact with remaining surface hydroxyls, which explains the complexity of the experimental NMR and IR data.

Introduction

The need for a sustainable and cleaner chemistry drives an important demand for highly efficient catalysts, which should be simultaneously active, selective for the desired product, and easily recycled. One successful direction toward this aim is to graft well-defined organometallic complexes on a large surface area oxide support, used as a solid ligand. This has been inspired by the success of homogeneous catalysis, which relies on the structure−reactivity relationship as a method to develop better catalytic systems, and which typically enters directly a catalytic cycle through the preparation of well-defined reaction intermediates.[1] This approach has already brought considerable success for olefin polymerization, hydrogenation, or metathesis.[2,3]

However, in heterogeneous catalysis, a fundamental understanding of the chemisorptive interaction and reaction of the metal−organic complex with the oxide surface is still lacking although Surface Organometallic Chemistry is designed to produce well-defined surface metallic species. The structural characterization of such a heterogeneous catalyst is indeed very difficult. This molecular understanding of the structure of surface complexes is critically needed if one wants to undertake a rational development of heterogeneous catalysts with a control on reaction selectivity. One first important question is the nature of the surface organometallic complex, in terms of molecular ligands remaining on the complex and number and type of bonds established with the oxide support (solid ligand). The cationic or neutral character of the surface metal species is also a key aspect for its catalytic properties, not easily accessible from experiment alone. Finally, one wants to understand which sites of the oxide surface are most appropriate for the grafting process. Do we really form a single well-defined surface/metal/ligands complex with a unique reactivity or can several species simultaneously be formed?

The choice of the oxide support plays a critical role. After years of research, we have shown that silica could be used as a tunable solid ligand, and the chemistry is now understood at a molecular level. Typically one can generate either monosiloxy, bissiloxy, and even in some cases trissiloxy surface complexes. These systems have been characterized by several methods (elemental analysis, IR, NMR, and EXAFS), and they have been used as catalyst precursors in several reactions (hydrogenation, polymerization, depolymerization, olefin metathesis, oxidation, and alkane metathesis). Typically, the siloxy substituent of the

[†] Laboratoire de Chimie, ENS Lyon.
[‡] Laboratoire de Chimie Organométallique de Surface, ESCPE Lyon.

(1) Copéret, C.; Chabanas, M.; Petroff Saint-Arroman, R.; Basset, J.-M. *Angew. Chem., Int. Ed.* **2003**, *42*, 156.
(2) Cornils, B.; Herrmann, W. A. *Applied Homogeneous Catalysis with Organometallic Compounds*, 2nd ed.; Wiley-VCH: 2002; Vol. 1.
(3) Cornils, B.; Herrmann, W. A. *Applied Homogeneous Catalysis with Organometallic Compounds*, 2nd ed.; Wiley-VCH: 2002; Vol. 2.

10.1021/ja0616736 CCC: $33.50

surface activates the metal center by generating more electrophilic metal centers,[1,4−6] but in some instances, it is necessary to use other supports such as alumina to obtain a gain in reactivity. Several hydrogenation, metathesis, and polymerization supported catalysts have been prepared, for which the alumina support is critical to obtain catalytic activity. For example, chemisorption of $[Zr(CH_2tBu)_4]$ on alumina provides an efficient olefin polymerization catalyst, while when supported on silica it is inactive.[7−9] Alumina has a richer chemistry than silica since it combines a variety of hydroxyl groups, with several modes of coordination, with a Lewis acid character on the aluminum. Various types of aluminum atoms are potentially present on the surface, from tri- to pentacoordinated, originating from the tetrahedral or octahedral cations of bulk γ-alumina.[10,11] The role of the aluminum Lewis centers for the chemisorptive interaction of the metal−organic complex and more generally the specificity of alumina for this process is still unclear. In some cases the formation of partially or fully cationic species has been proposed based on NMR spectroscopy.[7−9,12−21] Most recently, we have found that well-defined W carbyne complexes are inactive catalyst precursors for alkane metathesis when supported on silica, while they become active when supported on alumina.[22]

Whether in olefin polymerization or in alkane metathesis, the development of better catalysts is still a challenge, which requires a better understanding of the structure of active sites on this type of support. Therefore, we have decided to study the reactivity of alumina toward two organometallic reagents: $[Zr(CH_2tBu)_4]$ (**1**) and $[W(\equiv CtBu)(CH_2tBu)_3]$ (**2**). Our approach combines a characterization of the reaction products (mass balance analysis), a spectroscopic study of the surface species (NMR and in situ IR), and a quantum chemical exploration of reaction pathways and stable intermediates for the grafting of the metal−organic species on alumina. For an optimal consistency of the approach, the modeling part includes the simulation of spectroscopic NMR and IR data. It is based on a model of a partially hydrated γ-alumina surface which has been previously developed and validated.[11] Our specific aim is to compare the grafting mechanism for these two complexes on alumina, and a special focus is put on the existence (or non existence) of cationic metallic species and on the unique (or non unique) character of the formed surface entity.

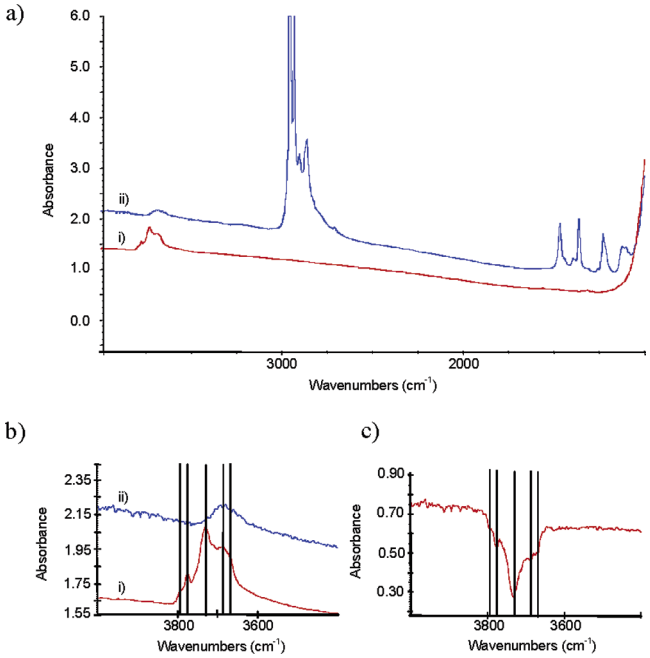

Figure 1. Monitoring the reaction of $[Zr(CH_2tBu)_4]$ and $Al_2O_{3-(500)}$ (100 mg) by IR spectroscopy: (a) (i) ($Al_2O_{3-(500)}$) and (ii) **1/Al$_2$O$_3$**. (b) Zoom in the $\nu_{(OH)}$ region [4000−3400 cm^{-1}] of (i) ($Al_2O_{3-(500)}$) and (ii) **1/Al$_2$O$_3$**. (c) Subtracted spectrum.

Results and Discussions

1. Analytical Results on the Reaction of $[Zr(CH_2tBu)_4]$ (1) with Alumina Partially Dehydroxylated at 500 °C. 1.1. In Situ IR Study. Monitoring by IR the reaction of an excess of **1**, $[Zr(CH_2tBu)_4]$, on an alumina disk partially dehydroxylated at 500 °C ($Al_2O_{3-(500)}$), shows that all the $\nu_{(OH)}$ vibrations are affected: the bands at 3795, 3776, and 3730 cm^{-1} (vide infra for assignment) have mostly disappeared (70%), whereas the bands at 3695 cm^{-1} are partially consumed (Figure 1). This is consistent with the existence of OH groups not accessible to **1**. Moreover, the characteristic bands in the 3000−2700 cm^{-1} and 1500−1300 cm^{-1} regions associated with the $\nu_{(CH)}$ and $\delta_{(CH)}$ of the perhydrocarbyl ligands around Zr have also appeared.

1.2. Mass Balance Analyses. After **1** is contacted at room temperature with γ-$Al_2O_{3-(500)}$, prepared from Boehmite, in pentane for 2 h, a solid **[1/Al$_2$O$_3$]$_B$** is obtained along with 1.8 equiv of $tBuCH_3$/grafted Zr. After this solid was washed and dried, elemental analysis shows the presence of Zr to the extent of 2.8%$_{wt}$, which corresponds to 0.31 mmol of Zr/g. As 1.8 equiv of $tBuCH_3$ evolved per grafted Zr, 1.8 OH are therefore consumed, and thereby 0.56 mmol of OH/g of alumina, in agreement with the disappearance of a large fraction (50%) of the surface hydroxyls (1.1 mmol of OH/g in the initial γ-$Al_2O_{3-(500)}$). Moreover, 11 C/Zr are found by elemental analysis, which is consistent with the quantity of $tBuCH_3$ evolved upon grafting. Similarly, using a γ-alumina from Degussa, 2.0 equiv of $tBuCH_3$ are formed per grafted Zr, about 50% of the OH are consumed, and the resulting complex contains around 11 carbons/Zr. Overall, the data are consistent with the formation of $[(Al_sO)_2Zr(CH_2tBu)_2]_{DA}$, **3**, as the major

(4) Ballard, D. G. H. *Adv. Catal.* **1973**, *23*, 263.
(5) Copéret, C. *New. J. Chem.* **2004**, *28*, 1.
(6) Solans-Monfort, X.; Clot, E.; Coperet, C.; Eisenstein, O. *J. Am. Chem. Soc.* **2005**, *127*, 14015.
(7) Tullock, C. W.; Tebbe, F. N.; Mulhaupt, R.; Ovenall, D. W.; Setterquist, R. A.; Ittel, S. D. *J. Polym. Sci., A* **1989**, *27*, 3063.
(8) Collette, J. W.; Tullock, C. W.; MacDonald, R. N.; Buck, W. H.; Su, A. C. L.; Harrell, J. R.; Mulhaupt, R.; Anderson, B. C. *Macromolecules* **1989**, *22*, 3851.
(9) Tullock, C. W.; Mulhaupt, R.; Ittel, S. D. *Makromol. Chem., Rapid Commun.* **1989**, *10*, 19.
(10) Digne, M.; Sautet, P.; Raybaud, P.; Toulhoat, H.; Artacho, E. *J. Phys. Chem. B* **2002**, *106*, 5155.
(11) Digne, M.; Sautet, P.; Raybaud, P.; Euzen, P.; Toulhoat, H. *J. Catal.* **2002**, *211*, 1.
(12) Burwell, R. L., Jr. *J. Catal.* **1984**, *86*, 301.
(13) Ballard, D. G. H. *Coord. Polym.* **1975**, 223.
(14) Ballard, D. G. H. *J. Polym. Sci., Polym. Chem. Ed.* **1975**, *13*, 2191.
(15) Toscano, P. J.; Marks, T. J. *J. Am. Chem. Soc.* **1985**, *107*, 653.
(16) Dahmen, K. H.; Hedden, D.; Burwell, R. L., Jr.; Marks, T. J. *Langmuir* **1988**, *4*, 1212.
(17) Gillespie, R. D.; Burwell, R. L., Jr.; Marks, T. J. *Langmuir* **1990**, *6*, 1465.
(18) Marks, T. J. *Acc. Chem. Res.* **1992**, *25*, 57.
(19) Ahn, H.; Marks, T. J. *J. Am. Chem. Soc.* **2002**, *124*, 7103.
(20) Buffon, R.; Leconte, M.; Choplin, A.; Basset, J.-M. *J. Chem. Soc., Dalton Trans.* **1994**, 1723.
(21) Jezequel, M.; Dufaud, V.; Ruiz-Garcia, M. J.; Carrillo-Hermosilla, F.; Neugebauer, U.; Niccolai, G. P.; Lefebvre, F.; Bayard, F.; Corker, J.; Fiddy, S.; Evans, J.; Broyer, J.-P.; Malinge, J.; Basset, J.-M. *J. Am. Chem. Soc.* **2001**, *123*, 3520.
(22) Le Roux, E.; Taoufik, M.; Coperet, C.; de Mallmann, A.; Thivolle-Cazat, J.; Basset, J.-M.; Maunders, B. M.; Sunley, G. J. *Angew. Chem., Int. Ed.* **2005**, *44*, 6755.

Scheme 1. Proposed Structures for the Reaction of **1** with $Al_2O_{3-(500)}$ (x = 1, 2, or 3)

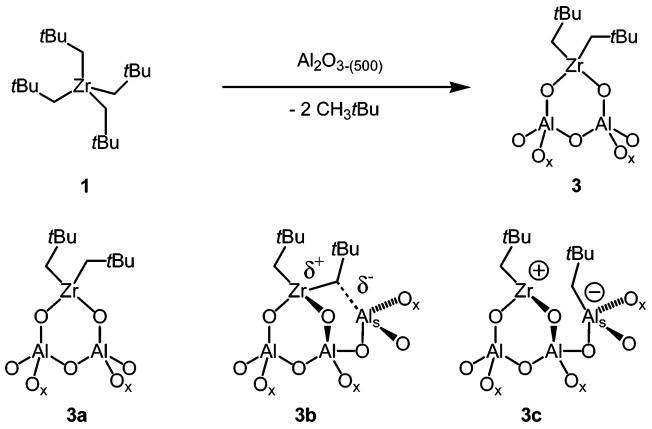

surface species, which contains 10 C/Zr and for which 2 equiv of tBuCH$_3$ are expected upon grafting (Scheme 1).

1.3. Solid-State NMR Spectroscopy. While no specific feature is observed on the ^{1}H NMR spectrum (a single broad peak centered at 1 ppm, Figure S1), the ^{13}C CP MAS solid state NMR spectrum of the unlabeled complex presents an intense peak at 32 ppm along with a shoulder at 29 ppm and two very broad peaks of low intensity at 84 and 26 ppm (Figure 2a). When the carbons directly attached to Zr in **1** are selectively ^{13}C labeled (33%), the two broad peaks at 26 and 84 ppm increase in intensity (Figure 2b), which is consistent with their attribution to methylene groups of tBuCH$_2$ fragments. Moreover, the signal at 84 ppm is very broad ($\Delta\nu_{1/2}$ > 4 kHz) and displays a shoulder at 99 ppm. The detailed attribution of NMR spectra will be presented later in the theoretical section 3.5.

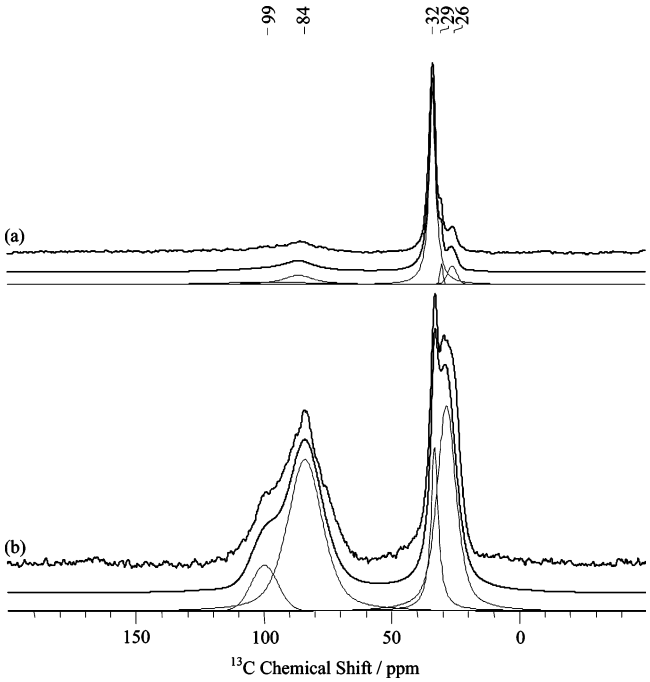

Figure 2. ^{13}C CP solid-state NMR spectrum of [Zr(CH$_2t$Bu)$_4$/Al$_2$O$_{3-(500)}$] recorded under MAS of 10 kHz. The simulated and deconvoluted spectra are shown below the experimental one. (a) **1/Al$_2$O$_{3-(500)}$**. The number of scans was 56 000, and the recycle delay was set to 1 s. A CP step of 2 ms was used. (b) **1*/Al$_2$O$_{3-(500)}$** (33% labeled ^{13}C on CH$_2$). The number of scans was 4096, and the recycle delay was set to 2 s. A CP step of 2 ms was used.

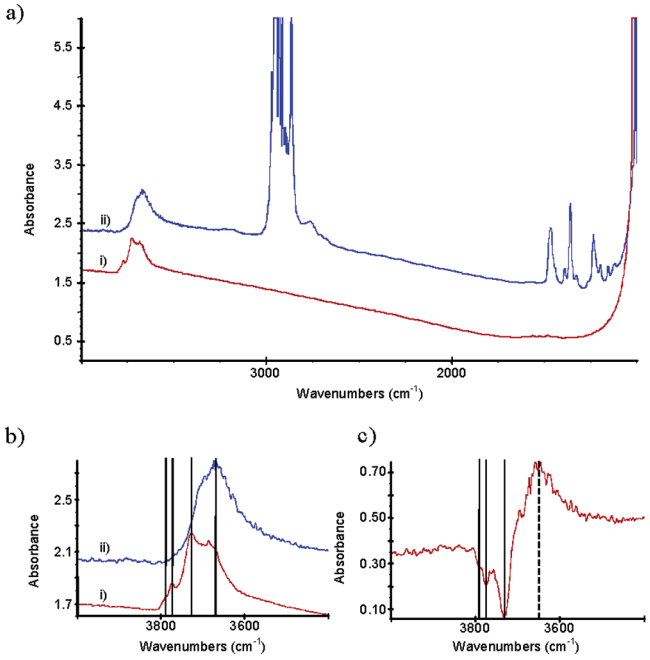

Figure 3. Monitoring the reaction of [W(≡CtBu)(CH$_2t$Bu)$_3$] and Al$_2$O$_{3-(500)}$ (100 mg) by IR spectroscopy: (a) (i) (Al$_2$O$_{3-(500)}$) and (ii) **2/Al$_2$O$_3$**. (b) Zoom in the $\nu_{(OH)}$ region [4000−3400 cm^{-1}] of (i) (Al$_2$O$_{3-(500)}$) and (ii) **2/Al$_2$O$_3$**. (c) Subtracted spectrum.

2. Analytical Results on the Reaction of [W(≡CtBu)(CH$_2t$Bu)$_3$] with Alumina Partially Dehydroxylated at 500 °C. 2.1. In Situ IR Study. Monitoring by IR the sublimation of an excess of **2**, [W(≡CtBu)(CH$_2t$Bu)$_3$], onto an alumina disk partially dehydroxylated at 500 °C (γ-Al$_2$O$_{3-(500)}$) shows that the $\nu_{(OH)}$ vibrations at 3795, 3776, and 3730 cm^{-1} disappeared (Figure 3), while some OHs appear as a large band centered at 3650 cm^{-1}. This is very different from what was observed during the grafting of [Zr(CH$_2t$Bu)$_4$] (**1**) (vide supra, disappearance of a large proportion of the OH bands and absence of bands shifted at lower frequencies). Moreover, the characteristic bands in the 3000−2700 cm^{-1} and 1500−1300 cm^{-1} regions associated with the $\nu_{(CH)}$ and $\delta_{(CH)}$ of the perhydrocarbyl ligands around W also have appeared.

2.2. Mass Balance Analyses. The reaction of a mechanical mixture of **2** and γ-Al$_2$O$_{3-(500)}$ (prepared from Boehmite) at 66 °C for 4 h generates 0.9 equiv of tBuCH$_3$/grafted W, and the corresponding solid is washed 3 times with pentane before drying under vacuum. Elemental analysis shows the presence of W to the extent of 3.8 wt %, which corresponds to 0.20 mmol of W/g. As 1 equiv of tBuCH$_3$ evolved per grafted W, 0.20 mmol of OH/g of alumina has been consumed, in agreement with the disappearance of a small fraction of the surface hydroxyls as evidenced by IR spectroscopy (consumption of 18% of 1.1 mmol of OH/g in the initial Al$_2$O$_{3-(500)}$). Moreover, an average of 14.7 C/W is found on the resulting solid by both elemental analysis and hydrogenolysis. Overall, the data are consistent with the formation of the surface complex [(Al$_s$O)W(≡CtBu)(CH$_2t$Bu)$_2$]$_{DA}$, **4** (Scheme 2), which contains 15C/W and for which 1 tBuCH$_3$ is expected during grafting.

2.3. Solid-State NMR Spectroscopy. The ^{1}H and ^{13}C solid-state NMR spectra of **2/Al$_2$O$_{3-(500)}$** display, respectively, a single peak centered at 1.0 ppm (Figure S2) and two peaks at 85 and 32 ppm (Figure 4a). When the compound **2** ^{13}C labeled on the carbon α to the metal was used to prepare **2/Al$_2$O$_{3-(500)}$**, the

Scheme 2. Proposed Structures for the Reaction of **2** with $Al_2O_{3-(500)}$ Based on Chemical Analyses

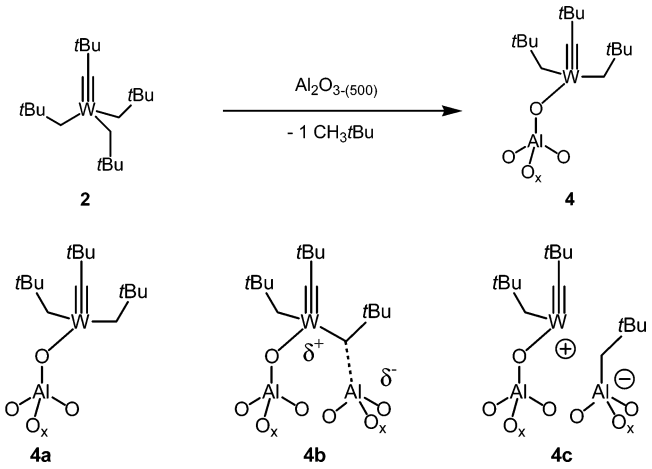

^{13}C CP/MAS NMR spectrum displays six major peaks at 318, 103, 95, 85, 52, and 32 ppm (Figure 4b, see deconvolution). By comparison with the ^{13}C NMR spectrum of the corresponding silica supported W complex,[24] it was clear that the carbyne ligand was left intact during grafting as evidenced by the peak at 318 and 52 ppm assigned, respectively, to the carbynic carbon (≡***C***tBu) and the quaternary carbon of the *t*Bu directly attached to this carbon (≡C***C***Me_3). Nonetheless, several species are possibly present as evidenced by the broad peak at 318 ppm and several peaks around 90 ppm (85, 95, and 103 ppm) and 30 ppm (32 and a shoulder at 29 ppm) attributed, respectively, to several types of methylene carbon (CH_2*t*Bu) and several *t*Bu groups. Based on what was proposed on alumina supported group 4 transition metal complexes,[18,21] we proposed earlier the presence of several surface species[22] such as neutral and possibly cationic surface species **4a**−**c** (vide infra for further comments and assignments).

3. Computional Study on the Reaction of Alumina with ZrR_4 (R = Me and CH_2*t*Bu) and W(CR′)(R) (R′ = R = Me and R′ = *t*Bu and R = CH_2*t*Bu). 3.1. Model Surface. Since γ-Al_2O_3 crystallites mainly expose (110) facets (between 70 and 83%), a periodic slab with (110) orientation was considered. Moreover the other surface present on the crystallite, (100), would not show any hydroxyl group at the considered pretreatment temperature and, hence, would not be reactive for grafting.[11] Ab initio atomistic thermodynamic calculations showed that in the experimental pretreatment conditions (500 °C) a coverage of 8.5 OH per nm^2 is present on the (110) surface,[11] which corresponds to three adsorbed H_2O molecules per surface unit cell (5.6 OH per nm^2 on γ-alumina). This OH density is slightly overestimated compared to experimental measurements (4 OH/nm^2).[25] On this most stable surface structure, several OH adsorption sites are present (see Figure 5a), and this termination reproduces reasonably well the diversity in the IR spectra of the real surface. It is hence a good sample to probe the reactivity of various types of OH group for grafting organometallic complexes.

It must be noticed that the complete description of the IR spectrum of realistic samples is not possible with a single orientation. Moreover, it has been proven that there is a nonhomogeneous repartition of hydroxyl groups on the surface,[26] which can explain both the overestimation of the hydroxyl density and the lack of some frequencies in this periodic model.

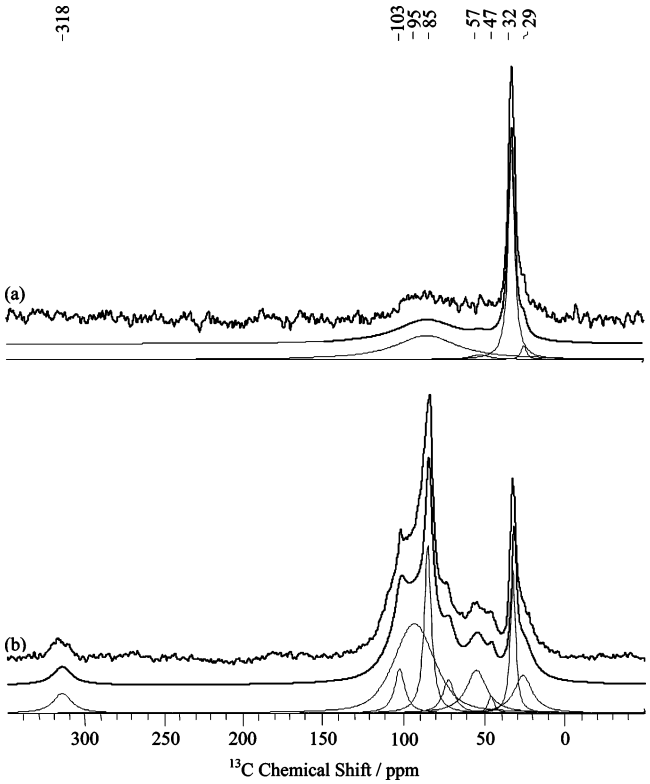

Figure 4. ^{13}C CP solid-state NMR spectrum of [W(≡C*t*Bu)(CH_2*t*Bu)$_3$/$Al_2O_{3-(500)}$] recorded under MAS of 10 kHz. The simulated and deconvoluted spectra are shown below the experimental one. (a) **2/$Al_2O_{3-(500)}$**. The number of scans was 55 000, and the recycle delay was set to 1 s. A CP step of 5 ms was used. (b) **2*/$Al_2O_{3-(500)}$** (30% labeled ^{13}C on CH_2). The number of scans was 55 000, and the recycle delay was set to 1 s. A CP step of 5 ms was used.

A first intrinsic measure of the reactivity of a hydroxyl group can be performed through the evaluation of its Lewis acidity, i.e., the capability of the proton to interact with a Lewis base without breaking the O−H bond. An example of such an interaction is shown in Figure 5c in the case of pyridine as a Lewis base. The adsorption energy of pyridine on the hydroxyl group is characteristic of its acidity: the higher the absolute value of adsorption energy, the more acidic the hydroxyl group. These adsorption energies are reported in Table 1 together with OH stretching frequencies prior to pyridine adsorption.

A clear trend emerges: the lower the Al atom coordination, the higher the vibration frequency for the OH coordinated to this Al atom. Hydrogen bonds affect drastically the vibrational properties of hydroxyl groups with a marked decrease of the stretching frequency. The adsorption strength of pyridine clearly correlates with the force constant of the hydroxyl group, the one with the largest Lewis acidity (i.e., the one which leads to the strongest pyridine adsorption) corresponding to the OH bonded to the tetrahedral Al (HO-μ^1-Al_{IV}). Conversely, the OH sites corresponding to a low OH frequency (μ^3 or hydrogen bonded) do not interact with pyridine (the molecule moves to

(23) Nedez, C.; Theolier, A.; Lefebvre, F.; Choplin, A.; Basset, J. M.; Joly, J. F. *J. Am. Chem. Soc.* **1993**, *115*, 722.
(24) Le Roux, E.; Taoufik, M.; Chabanas, M.; Alcor, D.; Baudouin, A.; Coperet, C.; Thivolle-Cazat, J.; Basset, J.-M.; Lesage, A.; Hediger, S.; Emsley, L. *Organometallics* **2005**, *24*, 4274.
(25) Zhang, W.; Sun, M.; Prins, R. *J. Phys. Chem. B* **2002**, *106*, 11805.
(26) Metivier, R.; Leray, I.; Roy-Auberger, M.; Zanier-Szydlowski, N.; Valeur, B. *New J. Chem.* **2002**, *26*, 411.

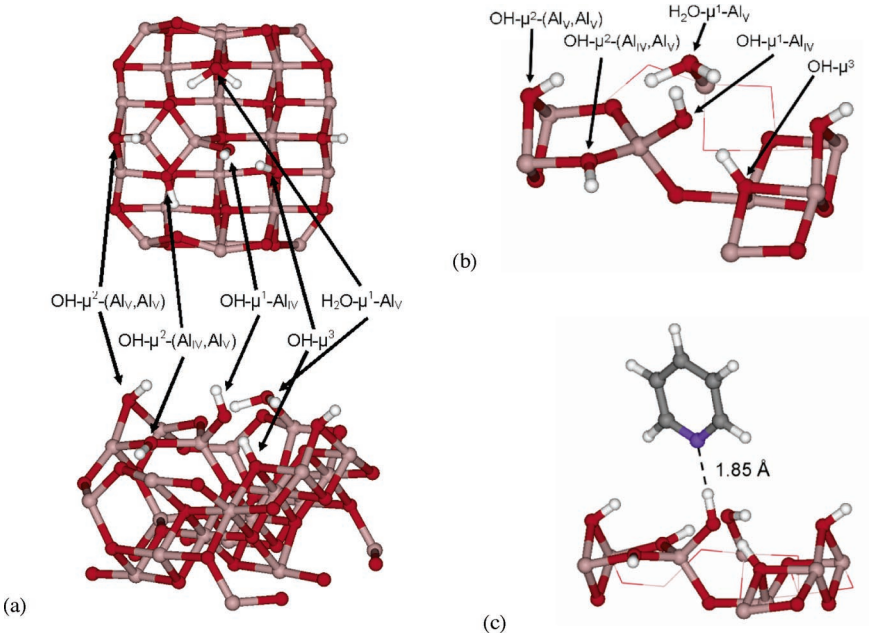

Figure 5. (a) Trihydrated γ-Al_2O_3 model surface. The roman numbers in index of Al is the coordination number. (b) Simplified representation of the same surface that will be used below for clarity. (c) Adsorption of pyridine on OH-μ^1-Al_{IV} group.

Table 1. Adsorption Energies (E_{ads}) of Pyridine on OH Groups and Stretching Frequencies (ν_{str}) of the Corresponding OH Groups Prior to Adsorption

OH group	E_{ads} (kJ mol^{-1})	ν_{str} (cm^{-1})
HO-μ^1-Al_{IV}	−40	3787
HO-μ^2-(Al_V,Al_V)	−31	3698
HO_2-μ^1-Al_V	−26 (free OH)	3490 (free OH)
		1243−1325 (O−H- - -O)
HO-μ^3-(Al_V,Al_{VI},Al_{VI})	*a*	2521
HO-μ^2-(Al_{IV},Al_V)	*a*	1528 (O−H- - -O)

[a] No adsorption on this site.

another site during geometry optimization). This suggests that they are probably not good candidates for grafting an organometallic complex so that they have not been considered later.

Upon pyridine adsorption, the calculated OH stretching frequency decreases by 600 cm^{-1} (800 cm^{-1} experimentally).[27] The calculated value is underestimated, but the trend is reproduced. Note that the frequencies are sensitive to weak interaction, which makes them difficult to calculate accurately by DFT.

3.2. Model Complexes. The complexes Zr(CH_2*t*Bu)$_4$ (**1**) and W(≡C*t*Bu)(CH_2*t*Bu)$_3$ (**2**) are too large for a systematic description of the grafting reaction path by quantum modeling. Therefore, the neopentyl and the neopentylidyne ligands have been, respectively, replaced by methyl and ethylidyne ligands (Figure 6). Nonetheless, to check the influence of the real ligands, a selected set of structures has been recalculated using the complete ligand structure. No structural data is available for these complexes, but the calculated bond lengths are in good agreement with those reported for similar molecular complexes.[28−30]

3.3. Thermodynamics of Grafting of Zr(CH_3)$_4$ (1m) on Alumina. Grafting of a tetrahedral organometallic complex on an alumina surface can provide several species. First, the d^0 metal center can coordinate to the oxygen atom of the surface hydroxyl, leading to a pentacoordinated metal center as presented in Figure 7a. In the case of Zr(CH_3)$_4$, such an intermediate on the HO-μ^1-Al_{IV} is slightly more stable (by 7 kJ.mol^{-1}) than the starting complex isolated from the surface, while it is isoenergetic for the other hydroxyl sites. These weakly bound precursors are probably not stable intermediates, if entropic effects are taken into account. Nonetheless, they hint to the grafting mechanism (vide infra), leading to the monoaluminoxy surface complex, (Al_sO)Zr(CH_3)$_3$ (**5m**), with the production of one CH_4 molecule (Figure 7b).

The grafting reaction is largely exoenergetic for the different hydroxyl sites (Table 2) and favored by 14−15 kJ/mol on HO-μ^1-Al_{IV} compared to HO-μ^2-(Al_V,Al_V) and H_2O-μ^1-Al_V. Note that the higher the hydroxyl group stretching frequency is, the more exoenergetic the grafting is, as observed for the coordination of pyridine. Therefore, the OH frequency can indeed be used as a probe for the capacity of an oxygen atom to react with a Lewis acid (a H atom or a metal center).

The grafting step on HO-μ^1-Al_{IV} provides **5m** $Al_sOZr(CH_3)_3$ for which the Zr−O distance (1.99 Å) compares well with experimental data.[21,31] The Al−O distance is not affected by the replacement of H by Zr(CH_3)$_3$, as a Lewis acid is replaced by another one.

We have subsequently studied the reaction of the surface complex **5m**, $Al_{IV}OZr(CH_3)_3$, obtained by the interaction with the most reactive hydroxyl, with adjacent Lewis acid sites and surface hydroxyls. The transfer of one methyl ligand onto an adjacent Al Lewis acid site can generate a partially cationic complex **6m** $Al_sOZr(CH_3)_2(\mu\text{-}CH_3)Al_s$, where the μ-CH_3 ligand lies between Zr and a Al_V atom (Figure 8a). Such a structure is 98 kJ mol^{-1} more stable than the monoaluminoxy neutral Zr complex **5m**, $Al_sOZr(CH_3)_3$. In **6m** $Al_sOZr(CH_3)_2(\mu\text{-}CH_3)Al_s$, the Zr complex is further stabilized by an oxygen atom of a

(27) Pichat, P.; Mathieu, M. V.; Imelik, B. *Bull. Soc. Chim. Fr.* **1969**, 2611.
(28) Churchill, M. R.; Youngs, W. J. *Inorg. Chem.* **1979**, *18*, 2454.
(29) Orpen, A. G.; Brammer, L.; Allen, F. H.; Kennard, O.; Watson, D. G.; Taylor, R. *J. Chem. Soc., Dalton Trans.* **1989**, S1.
(30) Schrock, R. R. *Chem. Rev.* **2002**, *102*, 145.
(31) Howard, W. A.; Parkin, G. *Polyhedron* **1993**, *12*, 1253.

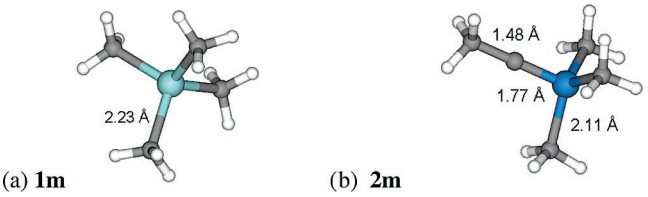

Figure 6. Optimized geometries of the model complexes: (a) $ZrMe_4$ (**1m**) and (b) W(≡CMe)Me_3 (**2m**).

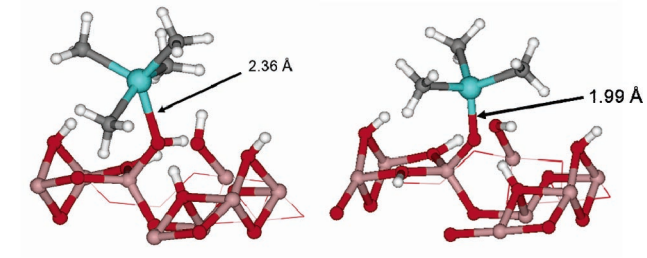

Figure 7. (a) Precursor state for grafting of $Zr(CH_3)_4$ on OH-μ^1-Al_{IV}. (b) Monoaluminoxy Zr species grafted on O-Al_{IV}, Al_{IV}O- $Zr(CH_3)_3$ (**5m**).

Table 2. Calculated Reaction Energy for the Grafting of $Zr(CH_3)_4$ on Different γ-Al_2O_3 Sites

surface site	E (kJ mol^{-1})
HO-μ^1-Al_{IV}	−201
HO-μ^2-(Al_V,Al_V)	−186
HO_2-μ^1-Al_V	−187

surface aluminoxane bridge, to compensate the loss of electrons from the shared ligand between Zr and Al.

Starting again from the monoaluminoxy surface complex **5m**, (Al_{IV}O)$Zr(CH_3)_3$, a second elimination of methane can occur by reaction with an adjacent Al_sOH, namely a HO-μ^1-Al_V which leads to a neutral bisaluminoxy species **3am**, $(Al_sO)_2Zr(CH_3)_2$ (Figure 8b). This reaction is exoenergetic: $\Delta_r E = -154$ kJ mol^{-1}. The energy is less favorable than for the first grafting step, probably because of geometric constraints on the surface. In fact, the OH groups are not placed in an ideal position to allow a perfect tetrahedral environment around the Zr atom.

The bisaluminoxy surface complex, $(Al_sO)_2Zr(CH_3)_2$ **3am**, or the partially cationic surface complex, $(Al_sO)Zr(CH_3)_2$-(μ-CH_3)(Al_s) **6m**, can further react with adjacent Lewis acid sites or an adjacent AlOH, respectively, to form a partially cationic bisaluminoxy surface complex **3bm** $(Al_sO)_2Zr(CH_3)$-(μ-CH_3)(Al_s) (Figure 9a). Both reactions are exoenergetic: $\Delta_r E = -80$ kJ mol^{-1} and -136 kJ mol^{-1}, respectively. Like in the partially cationic $(Al_sO)Zr(CH_3)_2(\mu$-$CH_3)(Al_s)$ complex **6m**, the coordination sphere of Zr is completed by an oxygen atom from an adjacent aluminoxane bridge.

Further reaction with a surface Al_sOH, namely a HO-μ^2-(Al_V,Al_V), to give a third equivalent of methane, whether starting from $(Al_sO)_2Zr(CH_3)_2$ **3am** or from the partially cationic surface complex, $(Al_sO)_2Zr(CH_3)(\mu$-$CH_3)(Al_s)$ **3bm**, is still possible, but the geometric constraint is even more important, which probably explains the lower energy gain: $\Delta_r E = -90$ kJ mol^{-1} (Figure 9b). In this case, the structure **7m**, $(Al_sO)_3Zr(CH_3)$, presents two quasi covalent Zr−O bonds (2.00 Å) and a slightly longer one (2.17 Å); the latter corresponds to a two-electron donation by an oxygen atom from the surface. Furthermore, there is a very long Zr−O bond (2.51 Å) of electrostatic character, the

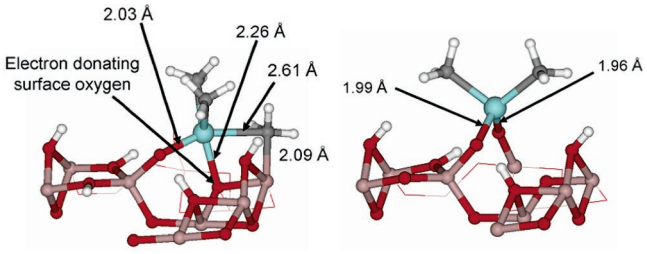

Figure 8. (a) The partially cationic monoaluminoxy Zr complex **6m**, $(Al_sO)Zr(CH_3)_2(\mu$-$CH_3)(Al_s)$. (b) The bisaluminoxy Zr surface complex **3am**, $(Al_sO)_2Zr(CH_3)_2$.

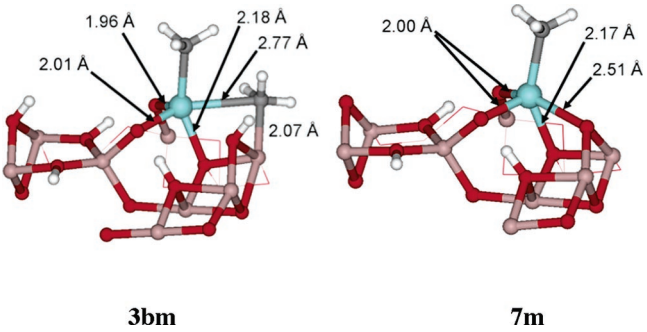

Figure 9. (a) The surface complex **3bm**, $(Al_sO)_2Zr(CH_3)(\mu$-$CH_3)(Al_s)$. (b) Trisaluminoxy Zr surface complex, $(Al_sO)_3ZrCH_3$ (**7m**).

oxygen atom between two Al and the Zr atoms being negatively charged. The trisaluminoxy surface complex, $(Al_sO)_3Zr(CH_3)$ **7m**, is slightly more stable than the partially cationic $Zr(CH_3)$-(μ-CH_3) complex **3bm**; however thermodynamics is not sufficient to understand the reactivity, and therefore pathways and activation barriers need to be addressed.

3.4. Kinetic Aspects for the Grafting of $Zr(CH_3)_4$ on Alumina. Since $Zr(CH_3)_4$ has only metal−carbon bonds and a d^0 configuration, only σ-bond metathesis between Zr−C and O−H has been studied for the Zr−O formation mechanism.

The energetic pathway for the three successive cleavages of the Zr−C bonds by surface hydroxyls resulting in the elimination of alkane molecules is reported in Scheme 3 including the possible rearrangement of surface species by reaction with adjacent Lewis acid sites. The structures of transition states are reported in Figure 10 with selected geometric data in Table 3.

The OH site that has been chosen to test the kinetic profile is on the tetrahedral Al site, HO-μ^1-Al_{IV}, because it has the largest interaction with pyridine and thereby it corresponds to the case where the proton is the most able to interact with a Lewis base (pyridine or an alkyl ligand) and probably the most reactive one. Additionally, the oxygen of this site has the greatest capability to interact with a Lewis acid (see the OH stretching frequency), and thus the formation of the metal−oxygen bond should also be favored. However, considering the large exothermicity of the reaction and the small difference in the stability of **5m** for the different hydroxyl sites, it is clear that the grafting reaction will also take place on the other sites (Table 2).

The first step (grafting **1m** → **5m**) is associated with the largest activation barrier ($\Delta_r E^{\ddagger} = 37$ kJ.mol^{-1}). The subsequent reactions are all easier except for the transformation of **3bm** $(Al_sO)_2Zr(CH_3)(\mu$-$CH_3)(Al_s)$ into **7m** $(Al_sO)_3Zr(CH_3)$, either

Scheme 3. Energetic Pathway for Three Successive Methane Eliminations Starting from **1m** + Al_2O_3[a]

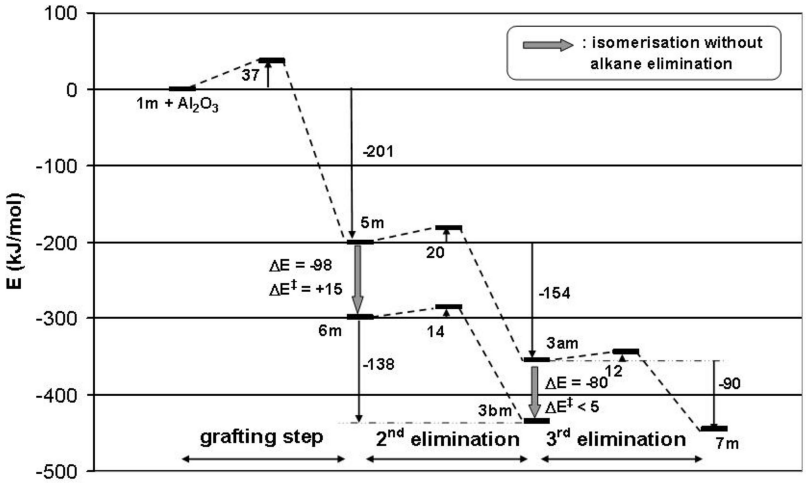

[a] Reactions with alkane elimination proceed horizontally, while surface isomerizations are indicated vertically with bold arrows.

through a direct pathway (which involves a σ-bond metathesis with the μ-CH_3 ligand) for which the activation barrier is > 150 kJ mol^{-1} or through a two-step reaction, which involves the reformation of **3am** $(AlsO)_2Zr(CH_3)_2$ followed by the reaction of a third OH group (E_a > 92 kJ mol^{-1}). The activation energy for the rearrangement of **5m** $(Al_sO)Zr(CH_3)_3$ into **6m** $(Al_sO)Zr(CH_3)_2(\mu\text{-}CH_3)Al_s$ via reaction with an adjacent aluminum is 15 kJ mol^{-1}. The geometry (Figure 10b) shows a very early transition state with a very low imaginary frequency along the reaction coordinate (61 cm^{-1}). Similarly, the activation energy for the rearrangement of **3am** $(Al_sO)_2Zr(CH_3)_2$ into **3bm** $(Al_sO)_2Zr(CH_3)(\mu\text{-}CH_3)(Al_s)$ is lower than 5 kJ mol^{-1}. Therefore, **3bm** $(Al_sO)_2Zr(CH_3)(\mu\text{-}CH_3)(Al_s)$ is likely to be obtained more rapidly than **7m** $(Al_sO)_3Zr(CH_3)$. This probably explains why the third Zr−C bond cleavage leading to a third equivalent of alkane is not observed experimentally even if it is slightly more favored on a thermodynamic basis.

In summary, the calculations show that the reaction of a Zr−CH_3 bond with surface Al_sOH is always exoenergetic and that the activation barriers are quite low (12−37 kJ mol^{-1}) except for a μ-CH_3 ligand. Moreover, they also show that the reaction with adjacent aluminum Lewis acid centers is probably faster than that with Al_sOH (E_a <14 kJ mol^{-1}), yielding partially cationic species. Therefore, the calculations would be consistent with the formation of **3bm** $(Al_sO)_2Zr(CH_3)(\mu\text{-}CH_3)(Al_s)$ with the release of 2 equiv of alkane in the gas phase as observed experimentally (vide supra).

To check the influence of the size of the ligand (replacement of CH_2tBu by methyl ligands) the activation barrier of the second Zr−C bond cleavage was evaluated with the full ligand. Note that the study with the neopentyl ligands requires quadrupling the size of the surface unit cell, which renders the calculation very CPU intensive, and therefore only certain reaction steps have been considered and only the activation barriers of the second elimination step have been evaluated. The activation barrier for the reaction of $(Al_sO)Zr(CH_2t\text{Bu})_3$ (**5m′**) with an adjacent Al_sOH to form $(Al_sO)_2Zr(CH_2t\text{Bu})_2$ (**3am′**) and tBuCH$_3$ is 26 kJ mol^{-1}, which is comparable to that obtained for the methyl system, i.e., 20 kJ mol^{-1}. Nonetheless, the use of the neopentyl ligands has two influences. First, the bond distances in the four-membered ring transition state are larger, probably because of greater steric repulsions (Table 3). Second, these ligands are better electron donors, which prevents the Zr−C bond from being lengthened too much by the steric effects. Hence, the energy of the transition state is not raised too much by the increase of the Zr−C bond length when changing methyl by neopentyl ligands. In any case, this study shows that the replacement of neopentyl ligands by methyl ligands in ZrR_4 does not dramatically affect the description of the elimination process.

In contrast, changing methyl for neopentyl ligands greatly affects the steps **5m** → **6m** and **3am** → **3bm**. In fact, while **5m** → **6m** is exoenergetic (−98 kJ mol^{-1}), the corresponding reaction with neopentyl ligands is endoenergetic (+38 kJ mol^{-1}) and in this case the neopentyl ligand cannot bridge Zr and Al like μ-CH_3 in **6m** $(Al_sO)Zr(CH_3)_2(\mu\text{-}CH_3)Al_s$: it is coordinated only on Al thus forming a cationic Zr complex.

The same trend is observed for **3am** → **3bm**, but the reaction remains exoenergetic (−23 kJ mol^{-1} for neopentyl vs −80 kJ mol^{-1} for methyl), and the neopentyl ligand is not a bridging ligand such as the case in **3bm** $(Al_sO)_2Zr(CH_3)(\mu\text{-}CH_3)(Al_s)$: there is a clear charge separation generating $\{[(Al_sO)_2Zr(CH_2t\text{Bu})^+][Al_s(CH_2t\text{Bu})^-]\}$ (**3c**, Figure 11).

It can be concluded from the kinetic study that **3bm** is the most probable model structure, obtained through **5m** and **3am** or through **5m** and **6m** in an equiprobable way. The third elimination yielding **7m** is excluded from a kinetic argument. While considering neopentyl ligands, the reaction path through the equivalent of **6m** is excluded, and the reaction goes through the equivalent of **5m** and **3am** giving $\{[(Al_sO)_2Zr(CH_2t\text{Bu})^+][Al_s(CH_2t\text{Bu})^-]\}$ (**3c**) as the most probable structure.

3.5. Comparison and Interpretation of Analytical and Computational Data for Zr. The proposed structure **3c** is in agreement with the mass balance analysis. To further refine the comparison between theory and experiment, we have calculated the ^{13}C NMR chemical shifts of the major surface species and compared them with experimental data (Table 4). Calculated NMR chemical shifts for $[Zr(CH_2t\text{Bu})_4]$ (**1**) are relatively close to the experimental data, especially for the carbon directly attached to Zr, which shows that the chosen basis set (IGLO-II combined with LANL2DZ) describes quite well the electronic properties of the Zr complexes.[32] For the proposed surface

(32) Ziegler, T.; Autschbach, J. *Chem. Rev.* **2005**, *105*, 2695.

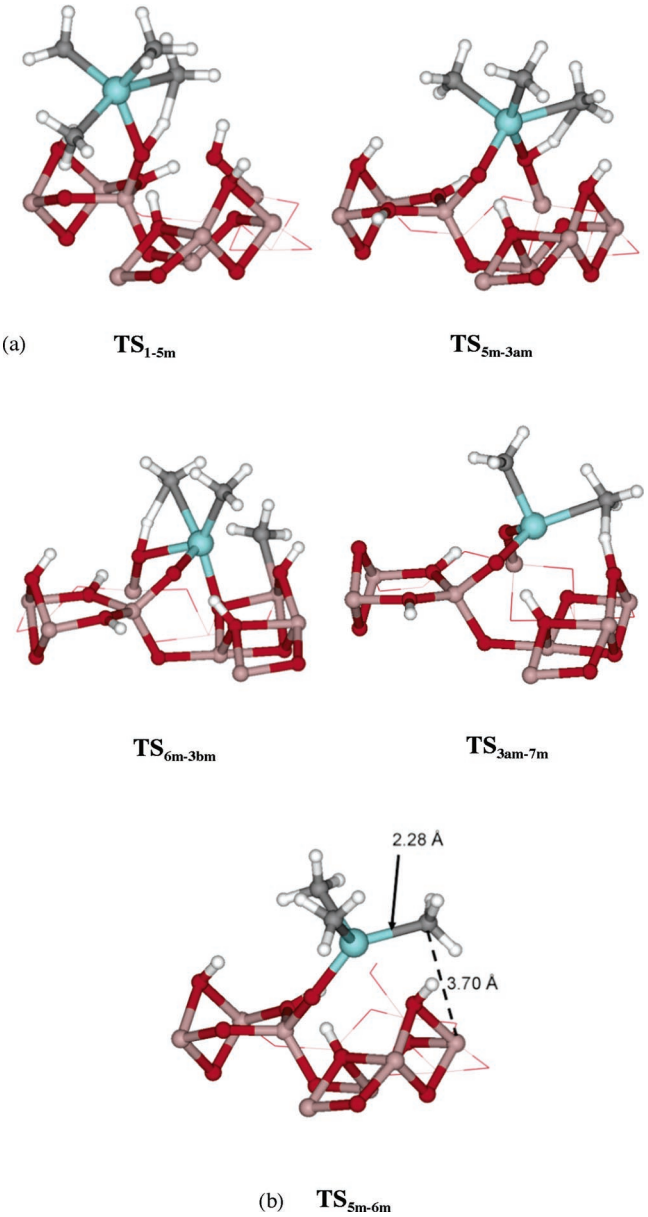

Figure 10. (a) Transition state structures for successive alkane eliminations in $Zr(CH_3)_4$ grafting. (b) Transition state structure for the rearrangement of **5m** $Al_sOZr(CH_3)_3$ to **6m** $Al_sOZr(CH_3)_2(\mu\text{-}CH_3)Al_s$.

Table 3. Distances (in Å) in the Four-membered Ring Transition States for Successive Alkane Eliminations for the Grafting of $Zr(CH_3)_4$ on Alumina

	grafting step	reaction with a second Al_sOH			with a third Al_sOH
	methyl ligands	methyl ligands on the neutral complex	methyl ligands on the cationic complex	neopentyl ligands	methyl ligands
	TS_{1m-5m}	TS_{5m-3am}	TS_{6m-3bm}	$TS_{5m'-3am'}$	TS_{3am-7m}
Zr−O	2.19	2.29	2.27	2.37	3.30
Zr−C	2.47	2.39	2.49	2.45	2.41
O−H	1.18	1.06	1.11	1.04	1.24
C−H	1.54	1.73	1.55	1.80	1.43

species $\{[(Al_sO)_2Zr(CH_2tBu)]^+[(Al_s)(tBuCH_2)]^-\}$, our analysis will be centered on the methylene carbon atoms which are direct neighbors of the metal Zr and Al atoms, and for which contributions have been highlighted in the experiment by ^{13}C labeling (Figure 2). In structure **3c**, the calculated chemical shift for the methylene carbon atoms attached to Zr and Al_{VI} are 86 and 90 ppm, respectively, which can be associated to the broad peak around 84 ppm and the shoulder at 99 ppm in the spectrum. For the $Zr(CH_2tBu)$ unit, the calculated upfield chemical shift compared to **1** is typical of the replacement of a carbon by a more electronegative atom (oxygen) in the coordination sphere of Zr.[33] Structure **3c** however does not account for the intense methylene peak at 26 ppm in the spectrum. In this geometry, the neopentyl ligand is bound to an octahedral Al atom. As surface aluminum atoms have several coordination geometries, we have also calculated a surface structure for which the neopentyl is borne by a tetrahedral Al_{IV} center. In this case, the calculated chemical shift for the methylene carbon is 25 ppm, in very good agreement with the data. This shows that neutral Zr neopentyl intermediates react with both Al_V and Al_{III} centers at the surface forming two types of $[Al_s(CH_2tBu)^-]$ species.

The analysis of experimental data in light of the model, which reproduces well the different features of the system, leads to the identification of the most probable surface structure for the grafted Zr complex. While initial grafting does not probably occur selectively on a tetrahedral Al site because of the high exothermicity of the process (along with the small difference of reaction energy, −186 to −201 kJ/mol) and the low activation barriers (12−37 kJ/mol), all the data are in agreement with the formation, as a major species, of a cationic bisaluminoxy mono-neopentyl zirconium complex bound to an aluminoxane bridge and in proximity of a neopentyl aluminate, the Al being either penta- (**3c**) or tetracoordinated.

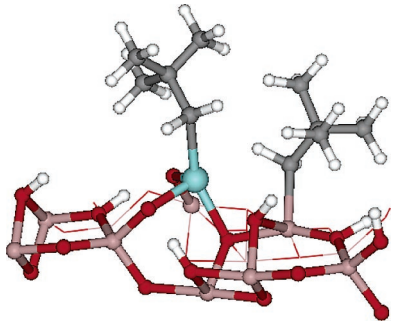

Figure 11. $\{[(Al_sO)_2Zr(CH_2tBu)^+][Al_s(CH_2tBu)^-]\}$ (**3c**) structure optimized on the model surface with the complete neopentyl ligands.

Table 4. Comparison of Calculated vs Experimental Carbon Chemical Shift for **1** and **3**

δ (ppm)		*C*H_2*t*Bu	CH_2*C*Me_3	*C*H_3
calculated for **1**		98	42	37
experimental for **1**[a]		102.6	35.4	34.7
calculated for **3c**	$ZrCH_2tBu$	86	40	40−41
	$Al_{VI}CH_2tBu$	90	49	36−46
	$Al_{IV}CH_2tBu$	25	36	33−41
experimental for **1**/Al_2O_3		99, 84, 26[c]	*b*	32, 29

[a] Recorded in C_6D_6. [b] Not observed. [c] Broad (see Figure 2 for details).

Table 5. Calculated Reaction Energy for the Grafting of $W(CCH_3)(CH_3)_3$ on Different γ-Al_2O_3 Sites

surface site	*E* (kJ mol^{-1})
HO-μ^1-Al_{IV}	−150
HO-μ^2-(Al_V,Al_V)	−139
HO_2-μ^1-Al_V	−130

(33) Berger, S.; Bock, W.; Frenking, G.; Jonas, V.; Mueller, F. *J. Am. Chem. Soc.* **1995**, *117*, 3820.

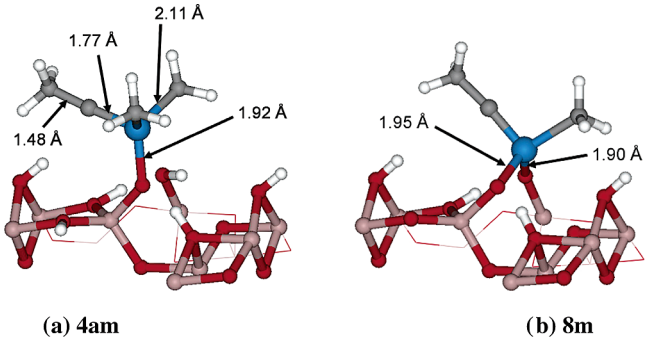

Figure 12. (a) Monoaluminoxy W surface complex on tetrahedral aluminoxy site, $(Al_{IV}O)W(CH_3)_2(\equiv CCH_3)$, **4am**. (b) Bisaluminoxy W surface complex **8m**, $(Al_sO)_2W(\equiv CCH_3)(CH_3)$ (remaining WC distances are not significantly modified by the reaction with the second Al—OH group).

After grafting, it is experimentally observed that some hydroxyl groups remain unreacted. Therefore, the stretching frequencies of these remaining hydroxyls have been calculated for the proposed final structure **3bm** $(Al_sO)_2Zr(CH_3)(\mu\text{-}CH_3)\text{-}(Al_s)$ and show no significant change compared to their original values as observed experimentally (see Figure 1).

3.6. Thermodynamics of Grafting of W(≡CMe)(CH$_3$)$_3$ on Alumina. For the $W(\equiv CCH_3)(CH_3)_3$ complex, the first step of the grafting process is quite similar to that for $Zr(CH_3)_4$. The major difference is that the precursor states are less stable than the complex isolated from the surface (by 3 to 7 kJ mol^{-1} depending on the Al_sOH site). Generally speaking, the tungsten−carbyne complex is more difficult to distort than the Zr complex because the formation of a pentacoordinated tungsten−carbyne complex by addition of a σ-donor ligand on $W(\equiv CCH_3)(CH_3)_3$ weakens the tungsten−carbon triple bond, hence giving less stable precursor states (vide infra). As already noticed in the case of $Zr(CH_3)_4$, this weakly bound precursor is probably not a stable intermediate, if entropic effects are taken into account.

The stability of the monoaluminoxy W surface complexes as a function of the surface Al_sOH site follows the same trend as that calculated for Zr complexes (Table 5): HO-μ^1-Al_{IV} > HO-μ^2-(Al_V,Al_V) > HO_2-μ^1-Al_V. The structure of the most stable monoaluminoxy complex is reported in Figure 12. The W−O distance reported in Figure 12 is in good agreement with X-ray diffraction data obtained for alkoxy tungsten complexes.[34]

Further reaction of **4am** $(Al_{IV}O)W(\equiv CCH_3)(CH_3)_2$ with an adjacent Al_sOH, leading to $(Al_sO)_2W(\equiv CCH_3)(CH_3)$ (**8m**) and a second equivalent of methane, is thermodynamically favorable (−90 kJ mol^{-1}), but less than for the first grafting step (−150 kJ mol^{-1}). Moreover and in contrast to Zr, all calculated cationic complexes, with a shift of a methyl group on a neighboring Al center, are less stable (≥ 49 kJ mol^{-1}) than **4am** $(Al_{IV}O)\text{-}W(CH_3)_2(\equiv CCH_3)$. This already infers that the formation of **4b**−**c** (Scheme 2), both cationic species, is probably unlikely in contrast to what we proposed earlier.[22]

3.7. Kinetic Aspects of W(CH$_3$)$_3$(CCH$_3$) Grafting. Grafting of $W(CH_3)_3(\equiv CCH_3)$ on alumina can take place via two reaction pathways. The first one goes through a σ-bond metathesis between W—CH_3 and O—H to form the O—W and H_3C—H bonds. The second one results from the addition of the hydroxyl group onto the carbyne to give a carbene, which undergoes an

Scheme 4. Two Possible Pathways for the Initial Grafting Step

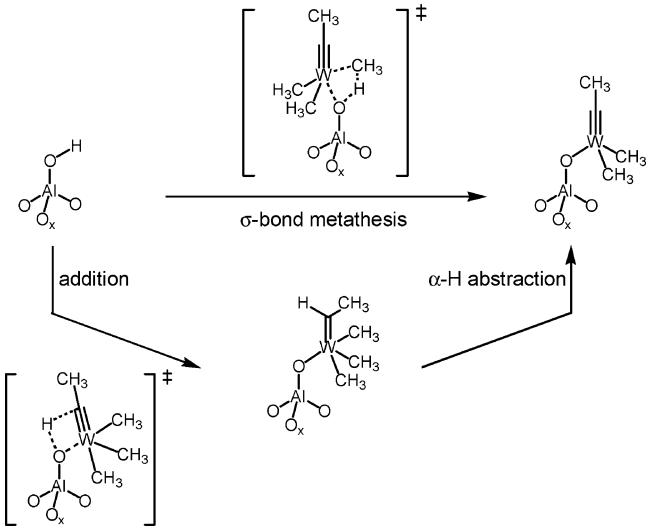

α-H-abstraction thus releasing an alkane molecule in the gas phase and restoring the W≡C bond (Scheme 4).

While the addition of an Al_sOH onto the carbyne requires going through a rather high activation barrier, i.e., $\Delta_rE^{\ddagger} = 126$ kJ mol^{-1}, the direct electrophilic cleavage of the W—C bond by Al_sOH gives a much lower activation energy (81 kJ mol^{-1}), which shows that grafting probably occurs via the latter pathway. The activation energy associated with the reaction of **4am** $(Al_{IV}O)W(CH_3)_2(\equiv CCH_3)$ with an adjacent hydroxyl group is only slightly lower (70 kJ mol^{-1}) than that of the grafting step (81 kJ mol^{-1}), but remains high (See Scheme 5 for the reaction path and Figure 13 for the corresponding TS). Note that, experimentally, alkylidyne complexes are in general not participating in the grafting process,[35] in contrast to alkyl and alkylidene ligands.[35−38] The comparison of the distances in Tables 3 and 6 shows that $\mathbf{TS_{2m-4am}}$ is later than $\mathbf{TS_{1m-5m}}$ which is reflected by the higher barrier.

As in the case of Zr, a test with the large neopentyl ligands on a quadruple unit cell has been performed. In contrast to Zr, the energy barrier for the second elimination increases substantially from 70 to 97 kJ mol^{-1}. In the case of W, the influence of realistic bulky ligands clearly disfavors the formation of the bisaluminoxy surface complex in contrast to Zr where the activation energy is little affected by changing the methyl by a neopentyl ligand. This probably explains why the second release of tBuCH$_3$ is not observed experimentally in contrast to what is observed during the grafting of the Zr complex, for which 2 equiv of tBuCH$_3$ are released. All these activation barriers are high compared to those obtained for Zr, and they are probably associated with the presence of the carbyne ligand, which is not prone to geometric deformation during the necessary formation of a pentacoordinated structure in the transition state. This is in agreement with the experimental results since the complete gratfing process is slower (greater experimental time and grafting temperature) for W than for Zr.

(34) Akiyama, M.; Chisholm, M. H.; Cotton, F. A.; Extine, M. W.; Haitko, D. A.; Little, D.; Fanwick, P. E. *Inorg. Chem.* **1979**, *18*, 2266.
(35) Chabanas, M.; Baudouin, A.; Copéret, C.; Basset, J.-M.; Lukens, W.; Lesage, A.; Hediger, S.; Emsley, L. *J. Am. Chem. Soc.* **2003**, *125*, 492.
(36) Dufaud, V.; Niccolai, G. P.; Thivolle-Cazat, J.; Basset, J.-M. *J. Am. Chem. Soc.* **1995**, *117*, 4288.
(37) Chabanas, M.; Quadrelli, E. A.; Fenet, B.; Copéret, C.; Thivolle-Cazat, J.; Basset, J.-M.; Lesage, A.; Emsley, L. *Angew. Chem., Int. Ed.* **2001**, *40*, 4493.
(38) Le Roux, E.; Chabanas, M.; Baudouin, A.; de Mallmann, A.; Copéret, C.; Quadrelli, E. A.; Thivolle-Cazat, J.; Basset, J.-M.; Lukens, W.; Lesage, A.; Emsley, L.; Sunley, G. J. *J. Am. Chem. Soc.* **2004**, *126*, 13391.

Scheme 5. Energetic Pathway for the Grafting of $W(\equiv CCH_3)(CH_3)_3$ on Alumina

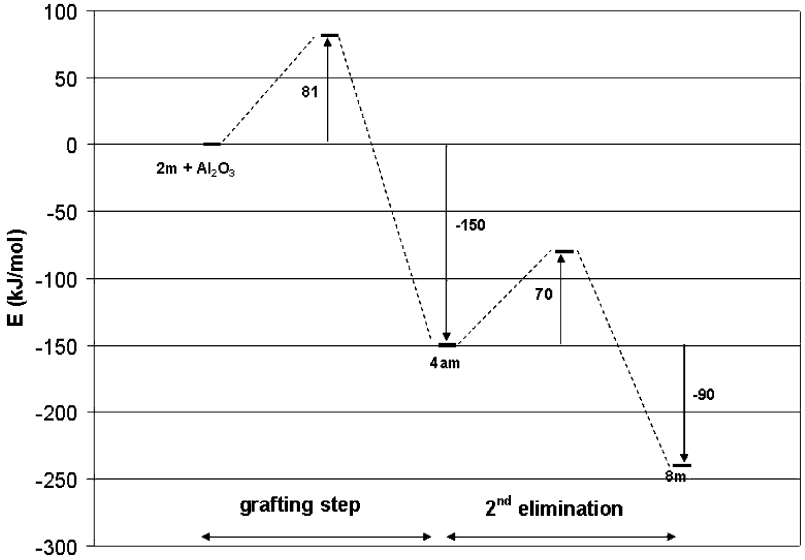

An orbital interaction diagram of the two situations (Figure 14), representing the starting complex and the pentacoordinated fragment, has been built to understand the behavior of **2** toward grafting. The surface hydroxyl is represented by a molecule of water for the pentacoordinated fragment. While the interaction between the p_x orbital on the carbyne fragment and the d_{xz} orbital on the metallic fragment is approximately the same for a $W(CH_3)_3$ and a $W(CH_3)_3(OH_2)$ fragment, the interaction of the p_y orbital on the carbyne fragment and the d_{yz} orbital on the metallic fragment is less favorable in the case of $W(CH_3)_3(OH_2)$ than $W(CH_3)_3$. The coordination of a fifth ligand to $W(CCH_3)(CH_3)_3$ therefore disrupts the π-bond system of the tungsten−carbon triple bond, thus destabilizing the complex.

3.8. Comparison of Analytical and Computational Data for W. From kinetic and thermodynamic considerations, **4am** seems to represent a good model for the grafted complex. This statement is further argued by a comparison between experimental and computational data, especially geometric features and IR and NMR data. First, the analogue of **4am** with real ligands (**4d**) has geometric features which agree very well with experimental EXAFS data (see Figure 15).[22]

To further evaluate the model, vibrational characteristics of hydroxyls interacting with **4am** $(Al_{IV}O)W(CH_3)_2(\equiv CCH_3)$ have been calculated. It appears that the stretching frequency of the remaining μ^2-OH is shifted compared to the bare surface, and the shift is associated with an extra interaction between this hydroxyl and the perhydrocarbyl ligands. For **4am** in which the OH is interacting with the π system of the carbyne, a large shift is obtained ($\Delta\nu = 70$ cm^{-1}, 3630 cm^{-1}), while, for **4am′**, a conformer of **4am** in which the OH interacts with the methyl ligand, a smaller shift is obtained ($\Delta\nu = 12$ cm^{-1}, 3688 cm^{-1}). Such a short contact between the carbyne and a surface hydroxyl group is specific of structure **4am** $(Al_{IV}O)W(\equiv CCH_3)(CH_3)_2$ (H···C distance of 2.78 Å) and does not appear in the case of **8m** $(Al_sO)_2W(\equiv CCH_3)(CH_3)$ (H···C distance of 3.40 Å). The calculated frequency shifts reproduce well the experimental data (see Figure 3) where a broad signal at 3650 cm^{-1} appears upon reaction of the tungsten complex with alumina, clearly indicating a perturbation of the remaining surface OH groups by the surface complex (such an interaction is not observed experimentally or by calculation in the case of zirconium).

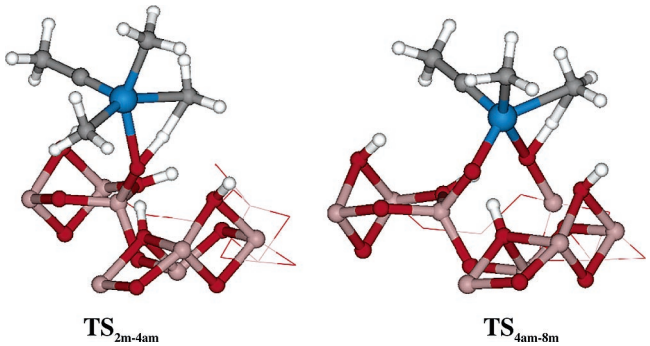

Figure 13. Transitions states structures $\mathbf{TS_{2m-4am}}$ and $\mathbf{TS_{4am-8m}}$ for successive alkane eliminations during the grafting of $W(CH_3)_3(\equiv CCH_3)$ on alumina (for geometric data, see Table 6).

Table 6. Geometric Parameters (in Å) in Four-membered Rings of Transition States in Successive Alkane Eliminations in $W(CH_3)_3(CCH_3)$ Grafting

	grafting step	reaction with a second Al_sOH	
	methyl ligands $\mathbf{TS_{2m-4am}}$	methyl ligands $\mathbf{TS_{4am-8m}}$	neopentyl ligands
W−O	2.29	2.23	2.29
W−C	2.33	2.33	2.29
O−H	1.25	1.27	1.27
C−H	1.43	1.42	1.42

The ^{13}C NMR spectrum of the W surface complex (Figure 4) displays six major peaks and was initially assigned to the presence of several species on the surfaces.[22] The presence of significant interactions between the hydrocarbon ligands and the surface OH groups, already seen in the ν_{OH} frequencies, opens a new interpretation where the multiple peaks are produced by a single surface W species, of **4a** type, but presenting several types of interactions between hydrocarbon ligands and surface OH groups. Experimentally, we observe a broadening of the carbynic signal and several types of methylene carbons: three peaks at 103, 90, and 85 ppm. We have therefore calculated the carbon chemical shifts of two conformers of the monoaluminoxy surface complex $(Al_sO)W(\equiv CtBu)(CH_2tBu)_2$ (Table 7): one showing an interaction of the carbyne with a vicinal hydroxyl group (**4d**, corresponding to **4am** for the model

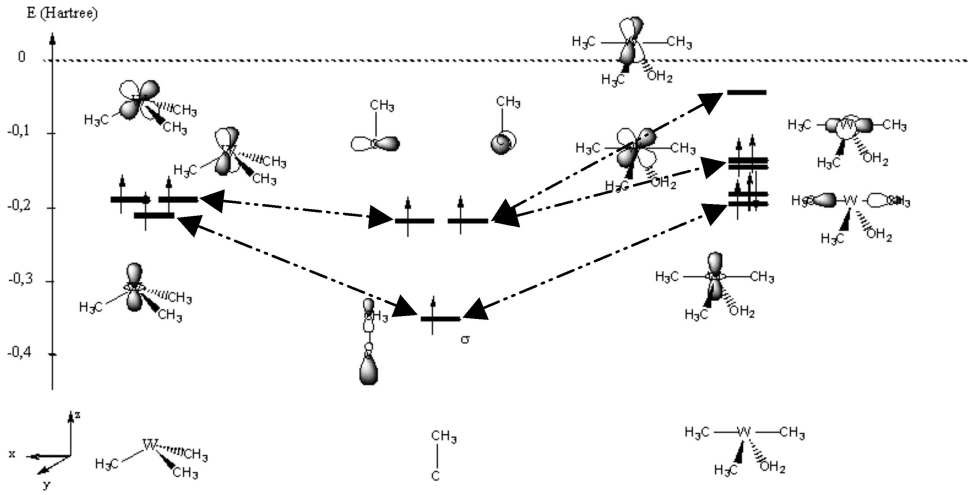

Figure 14. Orbital interaction diagram between CCH_3 and $W(CH_3)_3$ and $W(CH_3)_3(OH_2)$.

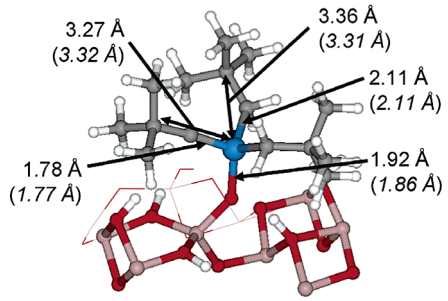

4d

Figure 15. Calculated and experimental (in italic letters) geometric features of the grafted tungsten complex **4d**.

Table 7. Comparison of Calculated vs Experimental Carbon Chemical Shifts for **2** and **4**[a]

δ (ppm)	≡*C*tBu	C*C*Me$_3$	CH$_2$*C*Me$_3$	*C*H$_2$tBu	*C*H$_3$
calculated for **2**	341	58	41	89	32−37
experimental data for **2**[a]	316	52	32	103	34
calculated for **4d**	312 (−29)	55 (−3)	38−39 (−3/−2)	85 (−4)	31−39
calculated for **4e**	336 (−5)	56 (−2)	38−39 (−3/−2)	70 (−19)[b] 85 (−4)	31−39
experimental data for **2**/Al_2O_3	318(2)[c]	52(0)[c]	*d*	103 (0)[c] 90 (−8)[c] 85 (−19)[c]	32,29

[a] The value in parentheses corresponds to Δδ between the ^{13}C calculated chemical shift for **2** and **4i (i = d** or **e)**. [b] Recorded in C_6D_6. [c] This calculated chemical shift corresponds to the one of the methylenes of the neopentyl ligand in interaction with a surface hydroxyl. [d] Broad peaks (see Figure 4 for details). [e] Not observed.

system) and the other having an interaction of one of its neopentyl ligands with a vicinal hydroxyl group (**4e**, corresponding to **4am′** for the model system) (Scheme 6).

First of all, the calculated ^{13}C chemical shifts for the carbons far from the metal centers are very accurate and do not vary significantly between complex **2** and the various surface complexes **4** (Table 7) as observed experimentally. Second, in the case of **4e**, the calculated chemical shift of the methylene carbon of the neopentyl ligand in interaction with the hydroxyl is shifted to 70 ppm ($\Delta\delta = -19$ ppm compared to the isolated complex **2**), while that of the remaining free neopentyl ligand is shifted upfield by only 4 ppm at 85 ppm ($\Delta\delta = -4$ ppm),

Scheme 6. Possible Interactions between a Surface Hydroxyl and the Ligands of $(Al_sO)W(\equiv C\,t\mathrm{Bu})(CH_2\,t\mathrm{Bu})_2$

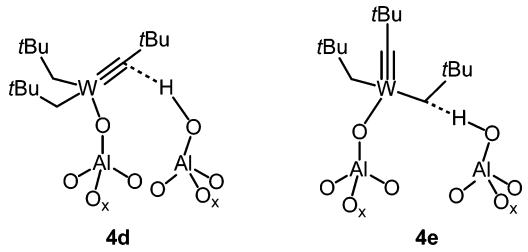

the carbynic carbon being shifted by only 5 ppm. This shows that the interaction with hydroxyls has a great influence on the chemical shift of the methylene carbon, which probably explains the upfield signal experimentally observed. Moreover, in the case of **4d**, for which the carbyne ligand interacts with adjacent hydroxyl groups, a large upfield shift of the carbynic carbon ($\Delta\delta = -29$) is calculated, while little influence is obtained for the methylene carbon ($\Delta\delta = -4$). Both types of interactions could explain the broadening of the carbynic signal. Thus, by comparing calculated and experimental data, we can propose that grafting **2** on alumina generates a monoaluminoxy surface species with several conformations, which interacts with residual surface hydroxyls as evidenced by IR spectroscopy, and which gives rise to a complex NMR spectrum. Such conformers of a single species allow a complete interpretation of the data. Moreover the combination of total energy calculations and experimental and calculated NMR data clearly demonstrates the absence of cationic species in the case of the grafting of the W carbyne complex.

Conclusion

A combination of physical chemical techniques and of quantum simulations has allowed a novel and complete characterization of the nature and structure of alumina single site catalysts. So far, silica supported organometallic complexes have been quite successfully characterized only from experimental physical chemical techniques, which have been the foundation of Surface Organometallic Chemistry (SOMC). As shown above, in the case of alumina, the surface chemistry can be so diverse that it has been necessary to include theoretical modeling as an essential tool of characterization in addition to the usual techniques of SOMC. The synergy between these approaches

has been illustrated by the understanding at a molecular level of the difference of reactivity of $[ZrR_4]$ and $[W(\equiv CR')R_3]$ complexes with alumina.

The first step of the reaction of ZrR_4 with an alumina partially dehydroxylated at 500 °C is an electrophilic cleavage of a Zr—C bond preferentially on $HO—Al_{IV}$ ($\Delta_r E = -201$ kJ/mol) through σ-bond metathesis with a low activation barrier ($E_a =$ 37 kJ/mol). This reaction gives $[(Al_sO)ZrR_3]$ along with one alkane molecule. In the case of $W(\equiv CR')R_3$, the first step is also an electrophilic cleavage of the W—R bond preferentially on $HO—Al_{IV}$ ($\Delta_r E = -150$ kJ/mol) to form $[(Al_sO)W(\equiv CR')R_2]$, but this reaction is associated with a much higher activation barrier ($E_a = 81$ kJ/mol). The lower reactivity of the W complex is due to the carbyne ligand, which hinders the necessary deformation of the complex for the approach of the Al_sOH toward the W—C bond. Although preferred on $HO—Al_{IV}$, the grafting reaction is also possible on other accessible OH groups such as $HO—(Al_v,Al_v)$, especially for the case of the Zr complex where the reaction barrier is low.

For Zr, the favored second step is the reaction of $[(Al_sO)ZrR_3]$ with an adjacent hydroxyl to give a neutral complex, $[(Al_sO)_2ZrR_2]$, and the evolution of a second molecule of alkane. This second step is still exoenergetic (−154 kJ/mol), its barrier is lower than that of the first step and is not affected by the size of the ligands (R = Me or CH_2tBu). This surface complex further reacts with the alumina surface in an almost barrierless process through the transfer of one of its alkyl ligands onto an adjacent Al_s Lewis center, giving a cationic surface complex $\{[(Al_sO)_2ZrR]^+[(Al_s)R^-]\}$. The alkyl transfer to give $[(Al_{IV})R^-]$ and $[(Al_{VI})R^-]$ has been confirmed by the combined use of ^{13}C CP-MAS solid-state NMR and chemical shift calculations. Moreover, this complete reaction pathway involves the formation of two alkane molecules per grafted Zr as observed experimentally.

The situation is completely different for the W carbyne complex. After the first step, the $[(Al_sO)W(\equiv CR')R_2]$ species is found to be nonreactive. Further reaction with surface hydroxyls involves a high reaction barrier (∼100 kJ/mol) for the real CH_2tBu ligand. This is in agreement with the evolution of a single alkane molecule in the reactive adsorption process. Moreover, transfer of an alkyl ligand to an adjacent Al center does not occur either as it involves the formation of unstable cationic species ($\Delta_r E = +50$ kJ/mol). This is also confirmed by the absence of typical ^{13}C NMR signals from surface alkyl aluminum species. Nonetheless, this neutral complex shows weak lateral interactions with the remaining adjacent surface hydroxyls as evidenced by a combination of IR spectroscopy and frequency calculations. It is noteworthy that the alumina supported W species, $[(Al_sO)W(\equiv CR')R_2]$, is in principle well-defined but that its ^{13}C NMR spectrum is complicated simply because this well-defined species interacts through its ligands (alkyl and carbyne) with different remaining hydroxyls present on the surface of alumina, thus providing different conformers, whose calculated NMR spectra are consistent with experimental data. This reflects the complexity of γ-alumina surfaces. In contrast, the zirconium complex, which has reacted with its surrounding hydroxyl groups and an adjacent aluminum, gives a fairly well-defined complex as evidenced by a rather simple NMR spectrum. It is a true cationic alkyl zirconium species, and this explains quite well why zirconium alkyls supported on alumina are active polymerization catalysts, while their corresponding silica supported analogues, neutral, are inactive.[7−9] The combination of theory and physical chemistry characterizations hence appears as a promising tool for the understanding, at a molecular scale, of well-defined surface catalytic species, enabling the rational design of highly efficient catalysts.

Computational Methods and Systems

The calculations were performed on the framework of density functional theory (DFT) using a periodic description of the system as implemented in the VASP code.[39,40] The generalized gradient approximation was used in the formulation of Perdew and Wang PW91.[41] Atomic cores were described with the projected augmented wave method (PAW) which is equivalent to an all electron frozen core approach.[42,43] The one electron wave functions are developed on a basis set of plane waves. With the selected PAW potentials, a cutoff energy of 275 eV is adequate and yields a converged total energy.

Brillouin zone integration was converged with a 331 k-point mesh generated by the Monkhorst−Pack algorithm.[44] Vibrational frequencies were calculated in the harmonic approximation by a numerical evaluation of the Hessian matrix. An anharmonicity term of 80 cm^{-1}, calculated previously on hydroxyl groups on boehmite, has been applied a posteriori.[45]

Chemical shifts have been evaluated with the GIAO method[46] implemented in the Gaussian03 code[47] at a DFT/B3LYP level.[48−51] The IGLO-II basis set[52] has been used for carbon and hydrogen. For other atoms, the Hay and Wadt effective core potential[53−55] has been used with the adapted LANL2DZ basis set. The chemical shift calculations have been performed on selected clusters. The interested reader will find more details in the Supporting Information in which a validation of computational parameters on well-defined molecules is also proposed.

Experimental Section

General Procedure. All experiments were conducted under strict inert atmosphere or vacuum conditions using standard Schlenk techniques. Solvents were purified and dried according to standard procedures. tBuCH$_2$MgCl was prepared from tBuCH$_2$Cl (98%, Aldrich) and Mg turnings (99%, Lancaster). [(1-^{13}C 33%) tBu^{13}CH$_2$MgCl] was prepared according to the literature procedure (It was prepared from a mixture of 1:2 [(1-^{13}C 99%) tBu^{13}CH$_2$MgCl] and unlabeled tBuCH$_2$MgCl. [(1-^{13}C 99%) tBu^{13}CH$_2$Cl] was prepared from (1-^{13}C 99%) H^{13}CONMe$_2$ (Cambridge Isotope Laboratories) and unlabeled tBuLi followed by reduction to the alcohol, chloration with a Vilsmeier reagent, and finally conversion to the Grignard with Mg).[35] [Zr(CH$_2t$Bu)$_4$] (**1**) and [(^{13}C 33%) Zr(CH$_2t$Bu)$_4$] (**1***) were prepared by alkylation of $ZrCl_4$ (Clariant, used as received) with tBuCH$_2$MgCl and [(1-^{13}C 33%) tBu^{13}CH$_2$MgCl], respectively, and were sublimed prior

(39) Kresse, G.; Furthmuller, J. *Comput. Mater. Sci.* **1996**, *6*, 15.
(40) Kresse, G.; Furthmueller, J. *Phys. Rev. B: Condens. Matter* **1996**, *54*, 11169.
(41) Perdew, J. P.; Chevary, J. A.; Vosko, S. H.; Jackson, K. A.; Pederson, M. R.; Singh, D. J.; Fiolhais, C. *Phys. Rev. B: Condens. Matter* **1992**, *46*, 6671.
(42) Bloechl, P. E.; Forst, C. J.; Schimpl, J. *Bull. Mater. Sci.* **2003**, *26*, 33.
(43) Bloechl, P. E. *Phys. Rev. B: Condens. Matter* **1994**, *50*, 17953.
(44) Monkhorst, H. J.; Pack, J. D. *Phys. Rev. B: Condens. Matter* **1976**, *13*, 5188.
(45) Raybaud, P.; Digne, M.; Iftimie, R.; Wellens, W.; Euzen, P.; Toulhoat, H. *J. Catal.* **2001**, *201*, 236.
(46) Ditchfield, R. *J. Chem. Phys.* **1972**, *56*, 5688.
(47) Pople, J. A. et al. *Gaussian 98*; Gaussian Inc.: Pittsburgh, PA, 1998.
(48) Becke, A. D. *Phys. Rev. A: At., Mol., Opt. Phys.* **1988**, *38*, 3098.
(49) Dickson, R. M.; Becke, A. D. *J. Chem. Phys.* **1993**, *99*, 3898.
(50) Becke, A. D. *J. Chem. Phys.* **1993**, *98*, 1372.
(51) Lee, C.; Yang, W.; Parr, R. G. *Phys. Rev. B: Condens. Matter* **1988**, *37*, 785.
(52) Kutzelnigg, W.; Fleischer, U.; Schindler, M. In *NMR basic principles and progress*; Springer: Berlin, 1990; Vol. 23, p 165.
(53) Hay, P. J.; Wadt, W. R. *J. Chem. Phys.* **1985**, *82*, 270.
(54) Hay, P. J.; Wadt, W. R. *J. Chem. Phys.* **1985**, *82*, 299.
(55) Wadt, W. R.; Hay, P. J. *J. Chem. Phys.* **1985**, *82*, 284.

to use.[56] [W(≡C*t*Bu)(CH_2*t*Bu)$_3$] (**2**) and [(^{13}C 30%) W(≡C*t*Bu)-(CH_2*t*Bu)$_3$] (**2***) were prepared with *t*BuCH_2MgCl and [(1-^{13}C 30%) *t*Bu$^{13}CH_2$MgCl], respectively, and were sublimed prior to use.[57] [W(≡C*t*Bu)(CH_2*t*Bu)$_3$/$Al_2O_{3-(500)}$] was synthesized according to the litterature procedure.[22] Elemental analysis was performed at the CNRS Central Analysis Service of Solaize (Zr, W) and at the University of Bourgogne (C).

Gas-phase analysis was performed on a Hewlett-Packard 5890 series II gas chromatograph equipped with a flame ionization detector and a KCl/Al_2O_3 on a fused silica column (50 m × 0.32 mm).

Infrared spectra were recorded on a Nicolet 550-FT by using an infrared cell equipped with CaF_2 windows, allowing in situ studies. Typically 16 scans were accumulated for each spectrum (resolution, 2 cm^{-1}).

All solid-state NMR spectra were recorded under MAS (ν_R = 10 kHz) on a Brüker Avance 500 spectrometer equipped with a standard 4-mm double-bearing probe head and operating at 500.13 and 125.73 MHz for ^{1}H and^{13}C, respectively. The freshly prepared samples were immediately introduced in the 4-mm zirconia rotor in a glovebox and tightly closed. Compressed air was used for both bearing and driving the rotors. Chemical shifts are reported in ppm downfield from $SiMe_4$ (±0.1 and 1 ppm for ^{1}H and ^{13}C NMR spectra, respectively). The typical cross-polarization sequence was used for the ^{13}C CP MAS NMR spectra: 90° proton pulse, cross-polarization step to carbon spins, and detection of the carbon magnetization under proton decoupling TPPM-15.[58] For the CP step, a ramp radio frequency (rf) field centered at ν^{CP} = 60 kHz was applied on protons, while the carbon rf field was matched to obtain optimal signal. The contact time for CP was set to 2 ms. An exponential line broadening of 80 Hz was applied before Fourier transform. All other details are given in the caption of figures.

Preparation of Partially Dehydroxylated Alumina at 500 °C, $Al_2O_{3-(500)}$. α-Boehmite monohydrate from Johnson Matthey (200 m^2/g) or γ-$Al_2O_{3-(500)}$ from Degussa C Aerosil (100 m^2/g) was calcined at 500 °C under N_2/O_2 flow overnight and then partially dehydroxylated at 500 °C under a high vacuum (1.34 Pa) for 12 h to give a white solid. The α-boehmite monohydrate from Johnson Matthey gave γ-$Al_2O_{3-(500)}$ having a specific surface area of 162 m^2/g and containing ca. 4.0 OH/nm^2 (1.1 mmol/g); ^{27}Al CP MAS NMR: δ_{Al} = 4 (3 Al, Oh), 62 ppm (1 Al, Td). γ-$Al_2O_{3-(500)}$ from Degussa C Aerosil gave a γ-$Al_2O_{3-(500)}$ having a specific surface area of 90 m^2/g and containing ca. 4.0 OH/nm^2 (0.6 mmol/g). ^{27}Al CP MAS NMR: δ_{Al} = 4 (3 Al, Oh), 62 ppm (1 Al, Td).

Grafting of Molecular Complexes on Alumina Monitored by IR Spectroscopy. Grafting of 1 (IR). Representative Procedure. Alumina (100 mg) was pressed into an 18-mm self-supporting disk, adjusted in sample holder, and put into a glass reactor equipped with CaF_2 windows. The support were prepared as described above, and **1** was then sublimed under high vacuum (1.34 Pa) at 80 °C onto the alumina disk. The solid was then heated at 65 °C for 2 h before the excess of complexes were removed by reverse sublimation at 80 °C and condensed into a tube cooled by liquid N_2, which was then sealed off using a torch. An IR spectrum was recorded at each step.

Grafting of 2 (IR). The same procedure was used for **2** by sublimation of **1** in place of **2**.

Preparation of [Zr(CH_2*t*Bu)$_4$/γ-$Al_2O_{3-(500)}$]$_D$ by Impregnation of [Zr(CH_2*t*Bu)$_4$] onto γ-$Al_2O_{3-(500)}$ from Degussa (Large Scale). Representative Procedure. A mixture of **1** (69 mg, 0.18 mmol) and γ-$Al_2O_{3-(500)}$ from Degussa (320 mg, 0.19 mmol AlOH) in pentane (8 mL) was stirred at 25 °C for 2 h. After filtration, the white solid was washed 3 times with pentane, and all volatiles were condensed into another reactor of known volume (> 6 L) in order to quantify *t*BuCH_3 released during grafting. The resulting light yellow powder was dried thoroughly under vaccum (1.34 Pa) to yield [**1**/γ-$Al_2O_{3-(500)}$]. Analysis by gas chromatography indicated the formation of 0.30 mmol of neopentane during grafting (2.2 *t*BuCH_3/Zr). ^{1}H MAS NMR: δ = 1.0 ppm. ^{13}C CP MAS NMR δ = 84 (weak), 32 and 26 ppm. Elemental analysis: 1.3%$_{wt}$ Zr, 2.3%$_{wt}$ C, 13 ± 2 C/Zr.

Preparation of [Zr(CH_2*t*Bu)$_4$/γ-$Al_2O_{3-(500)}$]$_B$ by Impregnation of [Zr(CH_2*t*Bu)$_4$] onto γ-$Al_2O_{3-(500)}$ Prepared from Boehmite (Large Scale). The same procedure as described above was used: A mixture of **1** (161 mg, 0.42 mmol) and γ-$Al_2O_{3-(500)}$ prepared from Boehmite as described above (590 mg, 0.65 mmol AlOH) in pentane (10 mL) was stirred at 25 °C for 2 h. Analysis by gas chromatography indicated the formation of 0.32 mmol of neopentane during grafting (1.8 *t*BuCH_3/Zr). ^{1}H MAS NMR: δ_H = 1.0 ppm. ^{13}C CP MAS NMR = 84 (weak), 32 and 26 ppm. Elemental analysis: 2.8%$_{wt}$ Zr, 4.1%$_{wt}$ C, 11 ± 2 C/Zr.

Preparation of [(^{13}C 33%) Zr(CH_2*t*Bu)$_4$/γ-$Al_2O_{3-(500)}$]$_D$ by Impregnation of [(^{13}C 33%) Zr(CH_2*t*Bu)$_4$] onto γ-$Al_2O_{3-(500)}$ (Large Scale). [1*/γ-$Al_2O_{3-(500)}$] was prepared using the procedure described above using **1*** (20 mg, 53 μmol) and γ-$Al_2O_{3-(500)}$ (109 mg, 65 μmolAlOH). ^{1}H MAS NMR δ: 1.0 ppm. ^{13}C CP MAS NMR δ: 99(*), 84(*), 32, 26(*).

Preparation of [W(≡C*t*Bu)(CH_2*t*Bu)$_3$/$Al_2O_{3-(500)}$]$_B$ by Impregnation of [W(≡C*t*Bu)(CH_2*t*Bu)$_3$] onto $Al_2O_{3-(500)}$ (Large Scale). An excess of **2** (311 mg, 0.66 mmol) and γ-$Al_2O_{3-(500)}$ prepared from Boehmite (1.8 g, 2 mmol OH) were stirred at 66 °C for 4 h. All volatile compounds were condensed into another reactor (of known volume) in order to quantify *t*BuCH_3 evolved during grafting. Analysis by gas chromatography indicated the formation of 0.21 ± 0.05 mmol of *t*BuCH_3 (0.9 ± 0.1 CH_3*t*Bu/W). Pentane (10 mL) was introduced into the reactor by distillation, and the solid was washed 3 times. After evaporation of the solvent, the resulting light brown powder was dried under a vacuum to yield [**2**/γ-$Al_2O_{3-(500)}$]. ^{1}H MAS NMR: δ_H = 1.0 ppm. ^{13}C CP MAS NMR = 85 (weak) and 32 ppm. Elemental analysis: 3.8%$_{wt}$ W, 3.6%$_{wt}$ C, 14 ± 2 C/W.

Preparation of [(^{13}C 30%) W(≡C*t*Bu)(CH_2*t*Bu)$_3$/$Al_2O_{3-(500)}$] by Impregnation of (^{13}C 30%) [W(≡C*t*Bu)(CH_2*t*Bu)$_3$] onto $Al_2O_{3-(500)}$ (Large Scale). [2*/γ-$Al_2O_{3-(500)}$] was prepared using the procedure described above using **2*** and γ-$Al_2O_{3-(500)}$. ^{1}H MAS NMR: δ_H 1.0 ppm. ^{13}C CP MAS NMR: 318(*), 103(*), 95(*), 85(*), 52, 32, 29. Elemental analysis: 4.7%$_{wt}$ W, 4.6%$_{wt}$ C, 15 ± 2 C/W.

Treatment under H_2 of the Solids. The solid was heated at 150 °C in the presence of a large excess of anhydrous H_2 (77 330 Pa). After 15 h, the gaseous product was quantified by GC.

Acknowledgment. We would like to thank BP Chemicals and the CNRS for financial support. F.B. is grateful to the Ministry of Research and Education for a predoctoral fellowship. We thank the Centre Informatique National de l'Enseignement Supérieur (CINES) at Montpellier and the Pôle Scientifique de Modélisation Numérique (PSMN) at ENS-Lyon for CPU time.

Supporting Information Available: More results on ^{1}H NMR spectroscopy and chemical shift modeling. This material is available free of charge via the Internet at http://pubs.acs.org.

JA0616736

(56) King, S. A.; Schwartz, J. *Inorg. Chem.* **1991**, *30*, 3771.
(57) Clark, D. N.; Schrock, R. R. *J. Am. Chem. Soc.* **1978**, *100*, 6774−6776.
(58) Hediger, S.; Meier, B. H.; Kurur, N. D.; Bodenhausen, G.; Ernst, R. R. *Chem. Phys. Lett.* **1994**, *223*, 283.